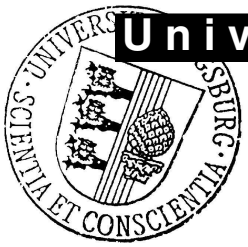

Universität Augsburg

Institut für Mathematik

Robert Azencott, Roland Glowinski, Jiwen He, Ronald H.W. Hoppe, Aarti Jajoo, Yipeng Li, Andrey Martynenko, Sagit Benzekry, Stuart H. Little, William A. Zoghbi

Optimal Diffeomorphic Matching in Biomedical Image Processing

Preprint Nr. 14/2010 — 29. Oktober 2010

Institut für Mathematik, Universitätsstraße, D-86135 Augsburg http://www.math.uni-augsburg.de/

Impressum:

Herausgeber:

Institut für Mathematik
Universität Augsburg
86135 Augsburg
`http://www.math.uni-augsburg.de/pages/de/forschung/preprints.shtml`

ViSdP:

Ronald H.W. Hoppe
Institut für Mathematik
Universität Augsburg
86135 Augsburg

Optimal Diffeomorphic Matching in Biomedical Image Processing

Robert Azencott[1,2], Roland Glowinski[2], Jiwen He[2], Ronald H.W. Hoppe[2,3], Aarti Jajoo[2], Yipeng Li[2], Andrey Martynenko[2], Sagit Ben Zekry, MD[4], Stuart H. Little, MD[4], and William A. Zoghbi, MD[4]

[1] Dept. of Math., Ecole Normale Superieure de Cachan, F-94230 Cachan, France
azencot@math.uh.edu
[2] Dept. of Math., Univ. of Houston, Houston, TX 77204-3008, U.S.A.
rohop@math.uh.edu
[3] Inst. of Math., Univ. of Augsburg, D-86159 Augsburg, Germany
hoppe@math.uni-augsburg.de
[4] The Methodist Hospital Research Institute, Houston, TX 77030, U.S.A
wzoghbi@tmhs.org

1 Introduction

3D imaging modalities such as CT, MRI, MRS, PET, SPECT, Ultrasound Echography, and X-Ray have become indispensable tools in clinical diagnosis and therapy planning. Automated 3D image registration provides a voxel to voxel matching of two 3D images of the same anatomical object obtained by different imaging modalities, at different times, or from different perspectives. A sufficiently good correspondence between reference and target images can be obtained on the basis of one or several matching quality criteria.
In general, image matching is achieved by an $\mathbb{R}^3$-diffeomorphism F matching two given bounded subdomains of the 3D voxel grid. In 2D or 3D-image registration, typical matching quality criteria involve the differences in image intensities at all pairs of matched voxels. The intensity matching cost is usually defined by a weighted sum of the image intensities over all voxels belonging to the domain of interest. Moreover, the diffeomorphism F can be assigned an elastic energy which measures the amount of spatial deformation. On this basis, optimal registration can be stated as a variational problem where a deformation F is sought that minimizes a linear combination of the elastic energy and the intensity matching cost.
Image registration methods have been initially designed for 2D-images. During the past decade, 3D-image registration based on volumetric data sets has attracted a lot of attention. A survey of image registration algorithms for biomedical applications can be found in [1].

The scenario which we consider in this paper is as follows: Given a 3D movie of a deformable anatomical shape $S(t) \subset \mathbb{R}^3, t \in I := [0,1]$, biomedical techniques enable the extraction of snapshots $S_j := S(t_j)$ at specific time frames $t_j, 0 \leq j \leq q$. The mathematical task is to find a family $F(\cdot,t) \in \mathrm{Diff}(\mathbb{R}^3), t \in I$, of time

dependent $\mathbb{R}^3$-diffeomorphisms

$$F(S_0;t_0) = S_0 \quad , \quad F(S_0;t_j) = \hat{S}_j \ , \ 1 \leq j \leq q,$$

which map the initial shape S_0 onto the shapes $\hat{S}_j$ at the time frames t_j such that for all $1 \leq j \leq q$ the shapes $\hat{S}_j$ are as close to S_j as possible.
In case of two snapshots S_0 and S_1, concepts based on diffeomorphic matching have been developed in [2–12]. The diffeomorphism $F(\cdot,t) = F^{v_t}, t \in I$, is generated by a time dependent flow v_t according to

$$\partial_t F(\cdot,t) = v_t(F(\cdot,t)) \ , \ t \in I, \tag{1a}$$

$$F(\cdot,0) = Id. \tag{1b}$$

The rigid constraint $F(S_0,t_1) = S_1$ is replaced by a soft constraint using suitably chosen geometric surface matching distances, and the resulting optimization problem is solved within a variational framework.
In particular, we will consider a generalization to arbitrarily many intermediary snapshots: Given $q+1$ snapshots $S_j, 0 \leq j \leq q$, at time instants $t_j \in [0,1], 0 =: t_0 < t_1 < \cdots < t_q := 1$, we want to compute a time dependent family of diffeomorphisms $F(\cdot,t) \in \mathrm{Diff}(\mathbb{R}^3), t \in [0,1]$, satisfying (1a),(1b) such that

$$E(v) + \sum_{j=1}^{q} \lambda_j D_j(F(S_0,t_j),S_j) \ \rightarrow \min,$$

where $E(v)$ is the elastic energy associated with the flow v, and $\lambda_j, D_j(\cdot,\cdot), 1 \leq j \leq q$, are regularization parameters and geometric surface matching distances, respectively.

The paper is organized as follows: Since an appropriate function space setting for the variational formulation of the optimal diffeomorphic matching problem is given by Reproducing Kernel Hilbert Spaces (RKHS), we provide a brief review of RKHS in section 2. The following section 3 is devoted to geometric surface matching distances, namely the Hausdorff distance and the Borel measure distance. In section 4, we provide the variational formulation, prove the existence of a minimizing diffeomorphic flow, and state the first order necessary optimality conditions. A semi-discretization in space featuring the approximation of the snapshots by point sets and the approximation of the Borel measures by Dirac measures is dealt with in 5 leading to optimal diffeomorphic point matching problems. In the subsequent section 6, we consider a time discretization of the optimality system which turns out to represent the first order necessary optimality conditions of a fully discrete optimization problem. On this basis, we develop a matching algorithm which is an inner/outer iterative scheme featuring a continuation method in the regularization parameters as outer iterations and a gradient method with Armijo line search as inner iterations. In the final section 7, we apply the matching algorithm to multiple snapshots of the mitral valve apparatus of the human heart and provide a documentation of numerical results illustrating the computational performance of the algorithm.

2 Reproducing Kernel Hilbert Spaces (RKHS)

Let H be a Hilbert space of functions on $\mathbb{R}^d$ with inner product $(\cdot,\cdot)_H$ and norm $\|\cdot\|_H$. A function $K : \mathbb{R}^d \times \mathbb{R}^d \to \mathbb{C}$ is said to be a reproducing kernel of H, if the following two conditions hold true:

$(RK)_1$ For every $x \in \mathbb{R}^d$, we have $K_x \in H$, where $K_x : \mathbb{R}^d \to \mathbb{C}$ is given by

$$K_x(y) = K(y,x) \quad , \quad y \in \mathbb{R}^d.$$

$(RK)_2$ For every $x \in \mathbb{R}^d$ and every $f \in H$ there holds

$$f(x) = (f, K_x)_H \quad , \quad x \in \mathbb{R}^d.$$

The Hilbert space H is said to be a Reproducing Kernel Hilbert space (RKHS), if there exists a reproducing kernel on H.
The kernel K is called Hermitian (positive definite), if for any finite set of points $\{y_1, \cdots, y_n\} \subset \mathbb{R}^d$ and any $\gamma_i \in \mathbb{C}, 1 \le i \le n$, there holds

$$\sum_{i,j=1}^{n} \bar{\gamma}_j \gamma_i \; K(y_j, y_i) \in \mathbb{R} \; (> 0).$$

Positive definite kernels uniquely determine the associated RKHS. Moreover, pointwise evaluations are continuous linear functionals [13].
We will consider positive definite translation invariant kernels. A kernel K is said to be translation invariant, if for any $a \in \mathbb{R}^d$

$$K(x-a, y-a) \;=\; K(x,y) \quad , \quad x, y \in \mathbb{R}^d.$$

By Bochner's theorem, they can be characterized as the Fourier transform of a finite positive Borel measure. A special class of translation invariant kernels are those given by radial functions. A function $K : \mathbb{R}^d \times \mathbb{R}^d \to \mathbb{C}$ is called radial, if there exists a function r on $\mathbb{R}_+$ such that

$$K(x,y) = r(|x-y|) \quad , \quad x, y \in \mathbb{R}^d.$$

In particular, Schoenberg's theorem [14] states that any continuous radial kernel admits the representation as a normally distributed positive Borel measure.
In the sequel, we will mainly deal with RKHS with reproducing Gaussian kernels. In this case, for any smooth function $f \in H$ the Frobenius norm of the Jacobian Df is bounded from according to

$$\|Df\|_F \le \frac{d}{\sigma} \|f\|_H,$$

where $\sigma > 0$ is the parameter from the associated Gaussian distribution.

3 Geometric surface matching distances

For the comparison of the snapshots $S_j, 1 \leq j \leq q$, with the deformed initial shapes $F(S_0, t_j)$ we use the following geometric distances:

- Hausdorff distance between two surfaces

$$D_H(F(S_0, t_j), S_j), \tag{2}$$

- Borel measure distance by identifying surfaces with bounded Borel measures

$$D^2_\Gamma(F(S_0, t_j), S_j). \tag{3}$$

3.1 Hausdorff distance

The Hausdorff distance between two bounded subsets $S, S' \in \mathbb{R}^3$ is given by

$$D_H(S, S') := \max\Big(h(S, S'), h(S', S)\Big), \tag{4}$$

where the Hausdorff disparity $h(S, S')$ is defined by means of

$$h(S, S') := \max_{x \in S} \min_{x' \in S'} |x - x'|.$$

The Hausdorff distance is not smooth. Instead, we use

$$\widetilde{D}_H(S, S') \ := \ h_{sm}(S, S') + h_{sm}(S', S), \tag{5}$$

where $h_{sm}(S, S')$ refers to a smoothed Hausdorff disparity.

3.2 Borel measure distance

We denote by $\mathrm{BM}(\mathbb{R}^3)$ the linear space of bounded Borel measures on $\mathbb{R}^3$ equipped with the inner product

$$\langle \mu, \mu' \rangle_\Gamma := \int_{\mathbb{R}^3} \int_{\mathbb{R}^3} \Gamma(x, x') \ d\mu(x) \ d\mu'(x'),$$

where $\Gamma(\cdot, \cdot)$ is a smooth, symmetric, and translation-invariant bounded positive definite kernel on $\mathbb{R}^3 \times \mathbb{R}^3$. We identify a bounded Borel subset $S \subset \mathbb{R}^3$ with a measure $\mu_S \in \mathrm{BM}(\mathbb{R}^3)$ induced on S by the Lebesgue measure of $\mathbb{R}^3$. The distance between two bounded Borel subsets $S, S' \in \mathbb{R}^3$ is defined by means of

$$D^2_\Gamma(S, S') := \|\mu_S - \mu_{S'}\|^2_\Gamma. \tag{6}$$

4 Variational formulation of the optimal diffeomorphic matching problem

We are now in a position to provide a variational formulation of the optimal diffeomorphic matching problem. We refer to $\mathcal{D}(I;V)$ as the space of all disparity functionals $D : L^2(I;V) \to \mathbb{R}_+$ of the form

$$D(v) = \Phi(F^v(\cdot,t_1),\cdots,F^v(\cdot,t_q)), \tag{7}$$

where $\Phi : \mathrm{Diff}(\mathbb{R}^3)^q \to \mathbb{R}_+$ is a continuous function.
We further denote by E the linear functional associating to a flow v its kinetic energy $E(v)$ according to

$$E(v) = \frac{1}{2}\int_0^1 \|v_t\|_V^2 \; dt, \tag{8}$$

which will be added to the disparity functional D as a regularizing term.
The optimal diffeomorphic matching problem then reads:
For a given disparity functional D, consider the objective functional J consisting of the weighted sum of the energy and the disparity functional with regularization parameter $\lambda > 0$, and minimize J over all admissible flows $v \in L^2(I;V)$ subject to the initial value problem for the evolution in time of the diffeomorphisms F describing the dynamic deformations of the initial snapshot: Find $v^* \in L^2(I;V)$ such that

$$J(v^*) = \inf_{v\in L^2(I;V)} J(v) \quad , \quad J(v) := E(v) + \lambda D(v), \tag{9a}$$

subject to

$$\partial_t F(\cdot,t) = v_t(F(\cdot,t)) \quad , \quad t \in I, \tag{9b}$$

$$F(\cdot,0) = Id. \tag{9c}$$

Theorem 1. *Assume that the embedding $V \subset W^{s,2}(\mathbb{R}^3), s > 5/2$, is continuous. Then, the optimal diffeomorphic matching problem* (9a)-(9c) *has a solution $v^* \in L^2(I;V)$.*

Proof. Let $\{v^n\}_{\mathbb{N}}$ be a minimizing sequence. Due to the boundedness of $\{v^n\}_{\mathbb{N}}$, there exist $\mathbb{N}' \subset \mathbb{N}$ and $v^* \in L^2(I;V)$ such that

$$\liminf_{n\to\infty} \|v^n\|_{L^2(I;V)} \le \|v^*\|_{L^2(I;V)}.$$

Denoting by $F^n(\cdot,t), F^*(\cdot,t) \in \mathrm{Diff}(\mathbb{R}^3), t \in I$, the unique flows solving (9b),(9c) with respect to v^n, v^*, the main part of the proof is to show that

$$F^n(\cdot,t) \to F^*(\cdot,t) \quad (n\to\infty) \; , \; t \in I,$$

uniformly on bounded subsets of $\mathbb{R}^3$ (see the proof of Theorem 3.2 in [15] for details). This implies $D(v^n) \to D(v^*)$ $(n \to \infty)$, and hence,

$$\lim\inf_{n\to\infty} J(v^n) \leq \lim_{n\to\infty} D(v^n) + \lim\inf_{n\to\infty} E(v^n) \leq D(v^*) + E(v^*) = J(v^*),$$

which allows to conclude.

The next result states the first order necessary optimality conditions.

Theorem 2. *In addition to the assumptions of Theorem 1, suppose that the functional $\Phi : C(\mathbb{R}^3)^q \to \mathbb{R}_+$ has Gâteaux derivatives $\partial_j\Phi \in M(\mathbb{R}^3), 1 \leq j \leq q$, where $M(\mathbb{R}^3)$ stands for the linear space of regular Borel measures.*
If $v^* \in L^2(I;V)$ is a solution of (9a)-(9c)*, then there exists a family $p^* = p^*_t, t \in I$, of vector valued Borel measures on $I \times \mathbb{R}^3$ satisfying the jump process*

$$-\partial_t p^*_t - b_{v^*,t} p^*_t = 0 \quad , \quad t \in (t_{j-1}, t_j), \tag{10a}$$

$$p^*_{t_q^+} = 0 \ , \ p^*_{t_j^-} = p^*_{t_j^+} + \lambda\partial_j\Phi(F^*(\cdot,t_j) \ , \ 1 \leq j \leq q, \tag{10b}$$

$$p^*_t + \rho_{t,v^*} = 0 \quad , \quad t \in I. \tag{10c}$$

Here, $b_{v,t} = (Dv_t(F(\cdot,t)))^T$, and $\rho_{t,v}$ is a vector valued Borel measure with density Kv_t.

Proof. We introduce the Lagrangian

$$L(F,v,p) := J(v) - \sum_{j=1}^{q} \int_{t_{j-1}}^{t_j} \langle p_t, \partial_t F(\cdot,t) - v_t(F(\cdot,t))\rangle_{M(\mathbb{R}^3),C(\mathbb{R}^3)} dt \tag{11}$$
$$- \langle p_0, F(\cdot,0) - Id\rangle_{M(\mathbb{R}^3),C(\mathbb{R}^3)},$$

where $p_t \in M(\mathbb{R}^3), t \in I$, is the Langrange multiplier coupling the constraints (9b) and (9c). If $v^* \in L^2(I;V)$ is a minimizing diffeomorphic flow with associated time dependent family of diffeomorphisms $F^*(\cdot,t)$ and multiplier p^*, the triple (F^*, v^*, p^*) is a critical point of the Lagrangian, i.e., there holds

$$L_F(F^*,v^*,p^*) = 0, \tag{12a}$$

$$L_v(F^*,v^*,p^*) = 0, \tag{12b}$$

$$L_p(F^*,v^*,p^*) = 0. \tag{12c}$$

In view of (7), we obtain

$$L_F(F^*,v^*,p^*) = \sum_{j=1}^{q} \lambda\partial_j\Phi(F^*(\cdot,t_j)) - \sum_{j=1}^{q-1}[p^*_{t_j}] - p^*_{t_q^-} + p^*_{t_0^+} - p_0$$
$$+ \sum_{j=1}^{q} \int_{t_{j-1}}^{t_j} \Big(\partial_t p^*_t + (Dv^*_t(F^*(\cdot,t)))^T p^*_{j,t}\Big) dt,$$

where $[p^*_{t_j}] = p_{t_j^-} - p_{t_j^+}, 1 \le j \le q$. It follows from (12a) that $p_0 = p_{t_0^+}$ and that (10a),(10b) are satisfied. Since the Gâteaux derivative of E at v is given by $\rho_{t,v} \in M(\mathbb{R}^3)$ with density Kv_t, (10c) is a consequence of (12b). Finally, (12c) results in (9b),(9c).

Remark 1. A controllability approach to diffeomorphic matching can be found in [16].

5 Discretization in space: diffeomorphic point matching

We consider a spatial discretization of the optimal diffeomorphic matching problem which results in an optimization problem for diffeomorphic point matching. We discretize the snapshots $S_j, 0 \le j \le q$, and the dynamically deformed surfaces $\hat{S}_j = F^v(S_0, t_j)$ by point sets

$$\begin{aligned} X_j &= \{x_1^j, \cdots, x_{N_j}^j\}, \\ \hat{X}_j &= F^v(X_0, t_j) = \{F^v(x_1^0, t_1), \cdots, F^v(x_{N_0}^0, t_j)\}. \end{aligned} \tag{13}$$

We denote by $x_n(t) = F^v(x_n^0, t_j)\ ,\ x_n(0) = x_n^0, 1 \le n \le N_0$, the trajectories emanating from x_n^0, i.e., the solutions of the initial value problems

$$\frac{d}{dt}\ x_n(t) = v_t(x_n(t))\ ,\ t \in [0,1], \tag{14a}$$

$$x_n(0) = x_n^0. \tag{14b}$$

We approximate the Borel measures associated with S_j and $\hat{S}_j$ by weighted sums of Dirac measures

$$\mu_{S_j} = \sum_{m=1}^{N_j} b_m^j\ \delta_{x_m^j} \quad , \quad \mu_{\hat{S}_j} = \sum_{n=1}^{N_0} a_n\ \delta_{x_n(t_j)} \quad , \quad 1 \le j \le q. \tag{15}$$

Setting $x(t) = (x_1(t), \cdots, x_{N_0}(t))^T, t \in (0,1)$, the disparity cost functional reads

$$D(v) = \sum_{j=1}^{q} \lambda_j\ D_j(x(t_j)) \quad , \quad D_j(x(t_j)) \ := \ \|\mu_{S_j} - \mu_{\hat{S}_j}\|^2_{K_{\sigma_j}}, \tag{16}$$

where we use individual regularization parameters $\lambda_j > 0$ and appropriately chosen radial Gaussian kernels $K_{\sigma_j}, 1 \le j \le q$.
We approximate the flow v_t by a linear combination of $K_{x_n(t)}, 1 \le n \le N_0$,

$$v_t(x) = \sum_{n=1}^{N_0} K_{\sigma_0}(x_n(t), x)\ \alpha_n(t) \quad , \quad x \in \mathbb{R}^3. \tag{17}$$

It follows that

$$\|v_t\|_V^2 = \sum_{n=1}^{N_0} \sum_{n'=1}^{N_0} K_{\sigma_0}(x_n(t), x_{n'}(t))\ \alpha_n^T(t)\alpha_n(t) \quad , \quad t \in [0,1],$$

Setting $\alpha(t) = (\alpha_1(t), \cdots, \alpha_{N_0}(t))^T \in \mathbb{R}^{dN_0}, t \in (0,1)$, and

$$A(x(t)) := \Big(K_{\sigma_0}(x_n(t), x_{n'}(t)) I_d\Big)_{n,n'=1}^{N_0} \in \mathbb{R}^{dN_0 \times dN_0}, \tag{18}$$

the optimal diffeomorphic point matching problem reads: Find $\alpha^* \in L^2(I; \mathbb{R}^{dN_0})$ and $x^*(t), t \in I$, such that

$$J(\alpha^*) = \inf_{\alpha} J(\alpha), \tag{19a}$$

$$J(\alpha) := \frac{1}{2} \int_0^1 \alpha(t)^T A(x(t)) \alpha(t)\ dt + \sum_{j=1}^{q} \lambda_j D_j(x(t_j)),$$

subject to

$$\frac{d}{dt}\ x^*(t) = A(x^*(t))\ \alpha^*(t) \quad , \quad t \in I, \tag{19b}$$

$$x^*(0) = x^0. \tag{19c}$$

The existence of a minimizing diffeomorphic flow can be shown along the lines of the proof of the previous Theorem 1, whereas the first order necessary optimality conditions state the existence of an adjoint state p^* which solves a final time problem for a backward in time dynamical system with jumps at the intermediate snapshot time instants $t_j, 1 \leq j \leq q-1$.

Theorem 3. *The discrete optimization problem* (19a)-(19c) *has a solution* $\alpha^* = \alpha^*(t), t \in I$. *If* $x^* = x^*(t), t \in I$, *is the associated trajectory, there exists a function* $p^* = p^*(t), t \in I$, *which solves the final time problem*

$$-\frac{d}{dt}\ p^*(t) = B(x^*(t), \alpha^*(t))^T \left(p^*(t) + \frac{1}{2}\ \alpha^*(t)\right)\ ,\ t \in (t_{j-1}, t_j), \tag{20a}$$

$$p^*(t_q^+) = 0\ ,\ p^*(t_j^-) = p^*(t_j^+) + \lambda_j\ \nabla D_j(x^*(t_j))\ ,\ 1 \leq j \leq q, \tag{20b}$$

Moreover, there holds

$$A(x^*(t))(\alpha^*(t) + p^*(t)) = 0\ ,\ t \in I, \tag{20c}$$

where the matrix $B(x^*(t), \alpha^*(t)) \in \mathbb{R}^{dN_0 \times dN_0}$ *in* (20a) *is given by*

$$B(x^*(t), \alpha^*(t)) \ = \ \nabla_x (A(x^*(t), \alpha^*(t))). \tag{21}$$

Proof. Introducing Lagrange multipliers $p(t) = (p_1(t), \cdots, p_{N_0}(t))^T \in \mathbb{R}^{N_0 d}$, $t \in I$, the Lagrangian associated with (19a)-(19c) is given by

$$L(\alpha, x, p) := J(\alpha) - \int_0^1 p \cdot \left(\frac{dx}{dt} - A(x(t))\alpha(t)\right)\ dt$$

$$= -\int_0^1 p \cdot \frac{dx}{dt}\ dt + \int_0^1 (p + \alpha/2) \cdot A(t,x)\alpha\ dt + \sum_{j=1}^{q} \lambda_j \mathrm{Disp}_j(x(t_j)).$$

The optimality conditions for a critical point (α^*, x^*, p^*) are given by:

$$L_\alpha(\alpha^*, x^*, p^*) = 0, \tag{22a}$$
$$L_x(\alpha^*, x^*, p^*) = 0, \tag{22b}$$
$$L_p(\alpha^*, x^*, p^*) = 0. \tag{22c}$$

Obviously, (22a) implies (20c), whereas (22c) gives rise to (19b),(19c). Using integration by parts, (22a) yields (20a),(20b).

6 Discretization in time and the matching algorithm

6.1 Discretization in time: fully discretized optimality system

For the discretization in time of the optimality system (19b),(19c),(20a),(20b), and (20c) we introduce the partition

$$\Delta_I := \bigcup_{j=1}^{q} \Delta_{I_j} \ , \ \Delta_{I_j} := \{t_{j-1} =: t^{L_{j-1}} < t^{L_{j-1}+1} < \cdots < t^{L_j} := t_j\},$$

where $\Delta_{I_j}, 1 \le j \le q$, are subpartitions of $I_j := [t_{j-1}, t_j]$. Setting $\Delta t^\ell := t^{\ell+1} - t^\ell, 0 =: L_0 \le \ell \le L := L_q$, the discretized optimality system reads

$$\frac{x^{\ell+1} - x^\ell}{\Delta t^\ell} = A(x^\ell \alpha^\ell \ , \ L_0 \le \ell \le L, \tag{23a}$$
$$x^0 = x^{(0)}, \tag{23b}$$
$$\frac{p^{(\ell-1)^+} - p^{\ell^-}}{\Delta t^{\ell-1}} = B(x^\ell, \alpha^\ell)^T (p^{\ell^-} + \alpha^\ell/2) \ , \ \ell = L_j, \cdots, L_{j-1} + 1, \tag{23c}$$
$$p^{L_q^-} = 0 \ , \ p^{L_j^-} = p^{L_j^+} + \lambda_j \nabla D_j(x^{L_j}) \ , \ 1 \le j \le q-1, \tag{23d}$$
$$A(x^\ell)(\alpha^\ell + p^{\ell^+}) \ , \ L_0 \le \ell \le L-1. \tag{23e}$$

Theorem 4. *Let J_{Δ_I} be the discrete objective functional*

$$J_{\Delta_I}(\alpha) = \frac{1}{2} \sum_{\ell=0}^{L-1} \Delta t^\ell \ (\alpha^\ell)^T A(x^\ell) \alpha^\ell + \sum_{j=1}^{q} \lambda_j D_j(x^{L_j}). \tag{24}$$

The discrete optimality system (23a)-(23e) *represents the first order necessary optimality conditions for the discrete optimization problem*

$$\min_\alpha J_{\Delta_I}(\alpha), \tag{25a}$$

subject to

$$\frac{x^{\ell+1} - x^\ell}{\Delta t^\ell} = A(x^\ell)\alpha^\ell \quad , \quad L_0 \le \ell \le L-1, \tag{25b}$$
$$x^0 = x^{(0)}. \tag{25c}$$

Proof. The assertion can be verified along the lines of the proof of Theorem 3.

6.2 Matching algorithm: inner/outer iterative scheme

The matching algorithm features an inner/outer iterative scheme with a continuation in the regularization parameters as an outer iteration and a gradient method with Armijo line search as inner iteration. The continuation is motivated by the following observation, where for simplicity we assume $\lambda_j = \lambda > 0, 1 \leq j \leq q$:
The regularization parameter provides a balance between the matching quality and the regularizing kinetic energy. The larger λ, the more emphasis is on the matching quality. However, the gradient method fails to converge for large λ, in particular, if the initial iterate is not close to a local minimum. A convenient remedy is continuation in the regularization parameter. A termination criterion for the continuation process is

$$D_j := \kappa\Big(\sum_{n=1}^{N_0}(d_n^j)^2\Big)^{1/2} < \vartheta \quad , \quad d_n^j := \min_{1\leq m\leq N_j}|x_n(t_j) - x_m(t_j)|, \tag{26}$$

where $\vartheta > 0$ is a given threshold and $0 < \kappa \leq 1$ (e.g., $\kappa = 0.9$).
With these prerequisites, the matching algorithm reads as follows:

Step 1: Initialization
Choose thresholds $\theta > 0, \vartheta > 0$, as well as $\boldsymbol{\gamma} > 1$ for continuation and $0 < \kappa \leq 1$.

Step 2: Initialization of the outer iteration
Choose an initial value λ_0 and set $\nu := 0$.

Step 3: Initialization of the inner iteration
Compute $\alpha_\nu^{(0)}$ by an appropriate initialization and set $\mu := 0$.

Step 4: Gradient method with Armijo line search

Step 4.1: Set $\mu := \mu + 1$ and compute $\alpha_\nu^{(\mu)}$ by gradient descent with Armijo line search.

Step 4.2: If the termination criterion $|\nabla J(\alpha_\nu^{(\mu)})| < \theta|\nabla J(\alpha_\nu^{(0)})|$ is satisfied, go to Step 5. Otherwise, go to Step 4.1.

Step 5: Termination of the outer iteration
If the termination criterion $D_j < \vartheta, 1 \leq j \leq q$, is satisfied, stop the algorithm. Otherwise, set $\nu := \nu + 1, \alpha_\nu^{(0)} := \alpha_{\nu-1}^{(\mu)},\ \lambda_\nu := \gamma\lambda_{\nu-1}$, and go to Step 4.

7 Application to optimal diffeomorphic matching of the mitral valve apparatus

7.1 The mitral valve apparatus of the human heart

The circulation of the blood flow in the human heart is controlled by four valves that guarantee a unidirectional flow through the chambers of the heart (cf. Figure

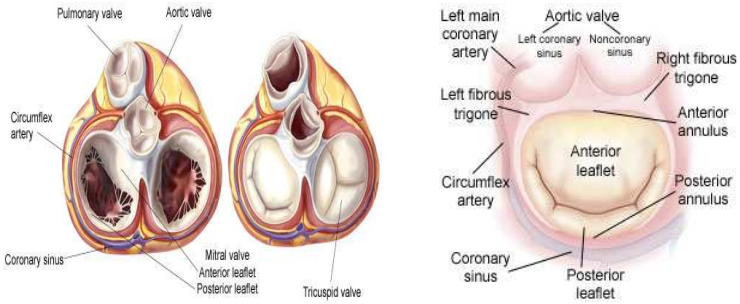

Fig. 1. Anatomy of the human heart (left) and the mitral valve (right)

1 (left)). The tricuspid valve between the right ventricle and the right atrium and the pulmonary valve between the right ventricle and the pulmonary artery control the flow of the venous blood from the body to the lungs. The mitral valve (bicuspid valve) between the left ventricle and the left atrium and the aortic valve between the left ventricle and the aorta control the flow of oxygen-rich blood from the lungs to the body.
The mitral valve apparatus (cf. Figure 1 (right)) consists of a saddle shaped annulus and two leaflets, the anterior and the posterior leaflet. According to the leaflet insertion, the annulus is divided into the anterior and the posterior annulus. The anterior annulus is connected to the right and left fibrous trigones, whereas the less developed posterior annulus is not connected to any fibrous structure. The semi-circular shaped anterior leaflet is attached to approximately 40 % of the annulus with its free boundary being indentation-free. On the other hand, the quadrangular shaped posterior leaflet has two well defined indentations that support the opening of the mitral valve during diastole.
Cardiovascular diseases due to anterior and/or posterior leaflet prolapse or mitral valve endocarditis often lead to a leaking valve and result in an abnormal heart rhythm. Such diseases require mitral valve repair or, in severe cases, mitral valve replacement.

We have applied the optimal matching algorithm to mitral valve annulus curves and mitral valve anterior as well as posterior leaflet surfaces based on NURBS snapshots obtained from echocardiographic data by a combination of optical flow extraction algorithms and surface tagging by medical experts (cf., e.g., [17, 18]). The number of intermediary heartbeat cycle time instants ranged from 3 to 8 with the time interval I covering either a half or a full heartbeat cycle.

7.2 Matching multiple snapshots of the mitral annulus

We first consider the matching of multiple snapshots for the mitral annulus which amounts to optimal diffeomorphic curve matching. We have used 5 successive

annulus snapshots with 42 points on the reference curve and approximately 500 points on the intermediaries and the target. As discrete time steps, we have chosen $\Delta t^{\ell} = 1/18$ starting from the initialization $\alpha = 0$.

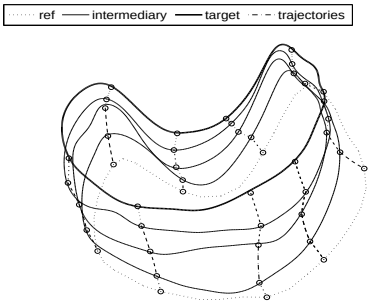

Fig. 2. Matching multiple snapshots of the mitral annulus at t = 1,3,5,7,10

The dotted curve in Figure 2 represents the reference curve. From bottom to top, the next 3 curves are the intermediary snapshots, and the last curve is the final target. The dashed lines are computed deformation trajectories for selected points on the reference curve.
The computational performance of the matching algorithm is evaluated by the convergence history reflected by the matching disparities both in case of smoothed Hausdorff matching and Borel measure matching. We will also display Pareto frontiers displaying the matching quality as a function of the regularizing kinetic energy.

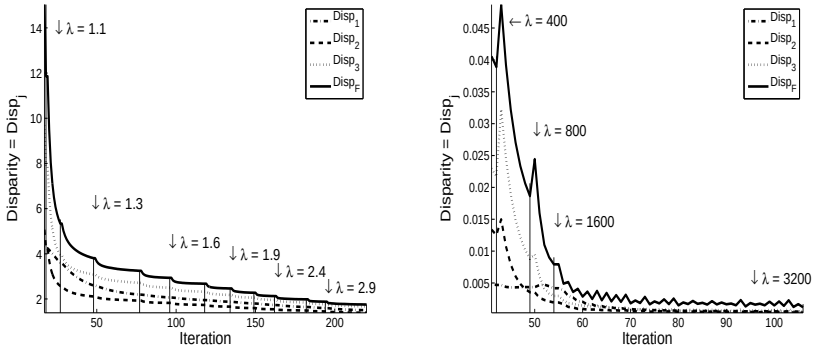

Fig. 3. Convergence history: smoothed Hausdorff disparities (left) and Borel measure disparities (right)

Figure 3 contains the convergence histories both for the individual Hausdorff disparities (left) and the Borel measure disparities (right). Each interval represents one step of the outer iteration for a specific value of the regularization parameter λ.

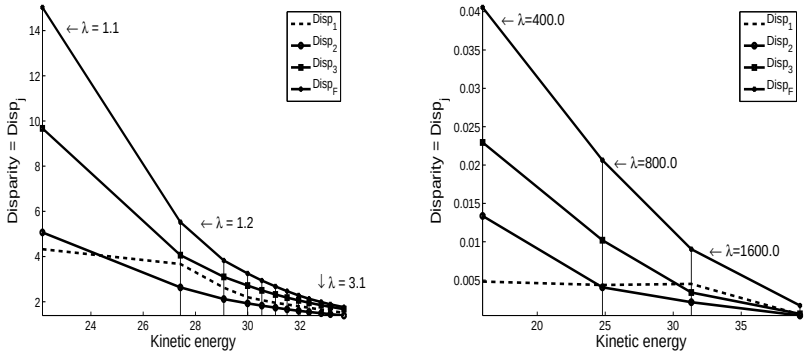

Fig. 4. Pareto frontiers: smoothed Hausdorff disparities (left) and Borel measure disparities (right)

The Pareto frontiers display the tradeoff between the matching quality and the kinetic energy. In the ideal case, points on the Pareto frontier represent weak Pareto optima for the pair of competing criteria, i.e., matching quality versus kinetic energy. For two person games, a weak Pareto optimum is a Pareto optimal strategy in the sense that there does not exist another strategy such that both players are better off with that strategy. Hence, a Pareto frontier should be a convex curve. The Pareto frontiers are shown in Figure 4 in case of smoothed Hausdorff disparities (left) and for Borel measure disparities (right). We see that the Pareto frontiers are convex except for the first intermediary snapshot at the beginning of the iterative process. The reason is that the algorithm improves the matching quality of the target first, followed by the intermediary snapshots in decreasing order.

7.3 Matching multiple snapshots of the mitral leaflets

We report on the performance of the matching algorithm applied to multiple snapshots of the anterior and the posterior leaflet. Given four snapshots S_0, S_1, S_2, S_3 of the anterior leaflet at time instants $0, 1, 5, 10$, we have implemented smoothed Hausdorff disparities featuring separate disparities for the boundary and the interior of each snapshot. For the initial discretization we have used 400 points on S_0 and approximately 1700 points on S_1, S_2 and S_3.
Figure 5 shows the reference surface (top left) and the computed deformations at time instants t=1,5,10 (top right and bottom). The Pareto frontiers for smoothed

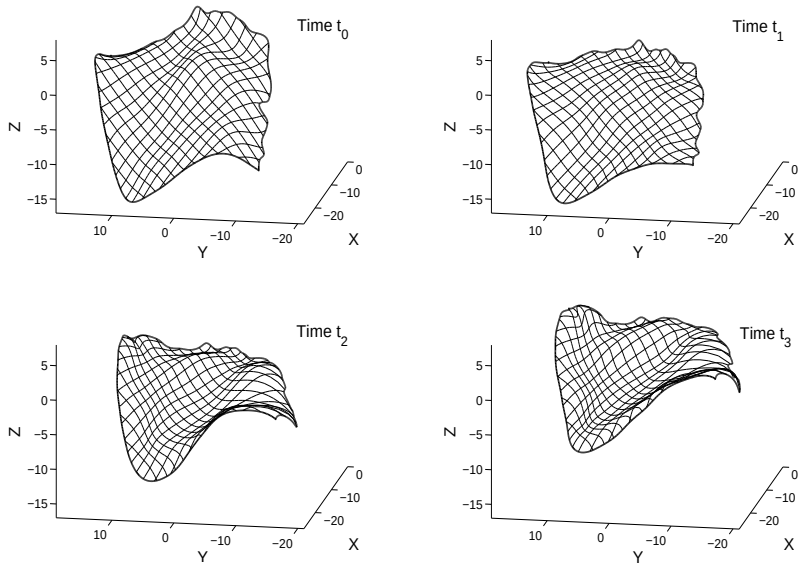

Fig. 5. Anterior leaflet: reference surface and computed deformations at time instants t=1,5,10 (from left to right and top to bottom)

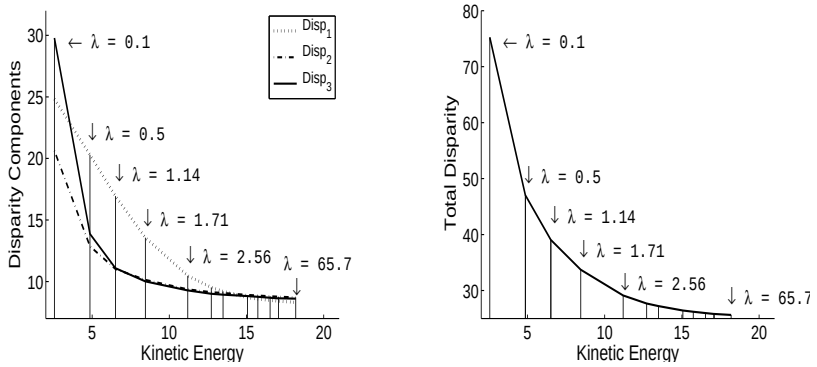

Fig. 6. Anterior leaflet: Pareto frontiers for individual Hausdorff disparities(left) and global Hausdorff disparity (right)

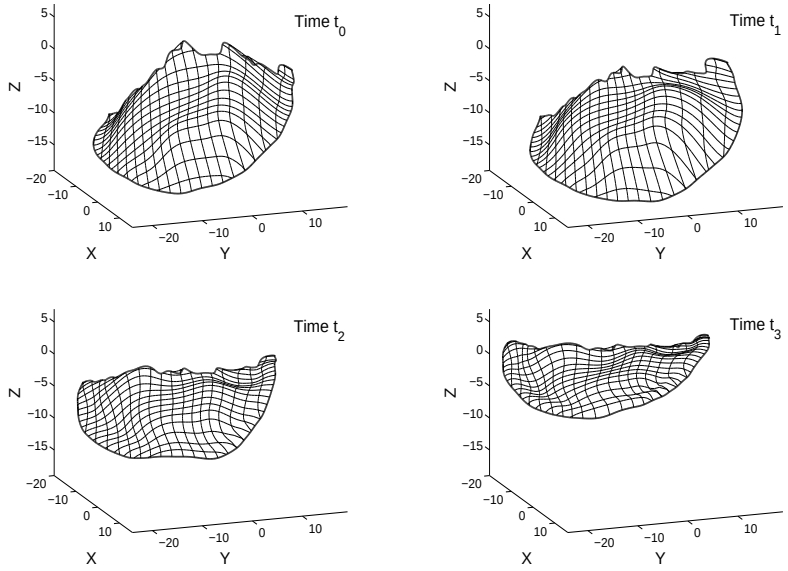

Fig. 7. Posterior leaflet: reference surface and computed deformations at time instants t=1,5,10 (from left to right and top to bottom)

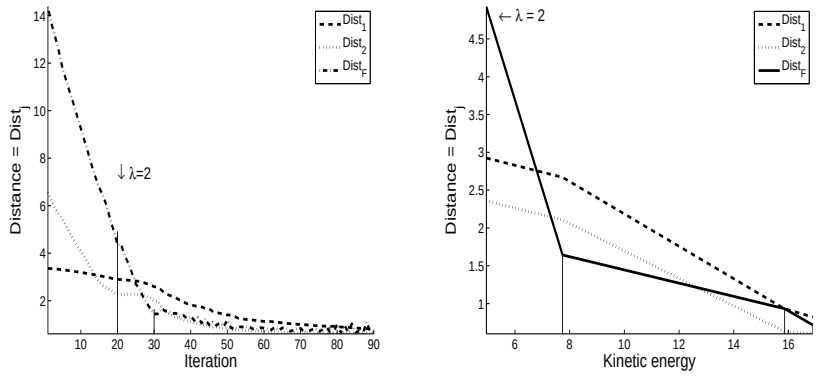

Fig. 8. Posterior leaflet: convergence history (left) and Pareto frontiers (right) for smoothed Hausdorff disparities

individual Hausdorff disparities are displayed in Figure 6 (left). For comparison, Figure 6 (right) contains the Pareto frontier in case of a smoothed global Hausdorff disparity.

The matching algorithm has been applied as well to four snapshots S_0, S_1, S_2, and S_3 of the posterior leaflet at the same time instants $0, 1, 5, 10$ based on smoothed Hausdorff disparities. In particular, for discretization we have used 250 points for the initial snapshot S_0 and and approximately 1100 points for the two intermediary snapshots and the target. Figure 7 displays the reference surface (top left) and the computed deformations at time instants t=1,5,10 (top right and bottom). The convergence history of the matching algorithm reflected by the geometric accuracy indicators is shown in Figure 8 (left), whereas Figure 8 (right) contains the Pareto frontiers.

Acknowledgements. The authors acknowledge support by the NSF under grant DMS-0811173 and The Methodist Hospital Research Institute, Houston, TX, USA.

References

1. Grenander, U., Miller, M.I.: Computational anatomy: an emerging discipline. Quart. App. Math. **56** (1998) 617–694
2. Beg, M., Miller, M., Trouvé, A., Younes, L.: Computing large deformations metric mappings via geodesic flows of diffeomorphisms. Int. J. Comp. Vis. **61** (2005) 139–157
3. Cao, Y., Miller, M.I., Winslow, R., Younes, L.: Large deformation metric mapping of vector fields. IEEE Trans. Med. Imaging **24** (2005) 1216–1230
4. Dupuis, P., Grenander, U., Miller, M.I.: Variational problems on flows of diffeomorphisms for image matching. Quart. Appl. Math. **56** (1998) 587–600
5. Glaunès, J.: Transport par difféomorphismes de points, de mesures et de courants pour la comparaison des formes et l'anatomie numérique (2005) PhD Thesis, Université Paris 13.
6. Glaunès, J., Qiu, A., Miller, M., Younes, L.: Large deformation diffeomorphic metric curve mapping. Int. J. Comp. Vision **80** (2008) 317–336
7. Glaunès, J., Vaillant, M., Miller, M.I.: Landmark matching via large deformation diffeomorphisms on the sphere. J. Math. Imaging Vis. **20** (2003) 179–200
8. Guo, H., Rangarajan, A., Joshi, S.: Diffeomorphic point matching. (2006) Handbook of Mathematical Models in Computer Vision, pp. 205-219, Springer, New York.
9. Miller, I., Trouvé, A., L.Younes: On the metrics and euler-lagrange equations of computational anatomy. Ann. Review of Biomedical Engineering **4** (2002) 375–405
10. Miller, M.I., Younes, L.: Group action, diffeomorphism and matching: A general framework. Int. J. Comp. Vis. **41** (2001) 61–84
11. Trouvé, A.: Diffeomorphisms groups and pattern matching in image analysis. Int. J. of Comp. Vis. **28** (1998) 213–221
12. Younes, L.: Computable elastic distances between shapes. SIAM J. Appl. Math. **58** (1998) 565–586

13. Aronszajn, N.: Theory of reproducing kernels. Trans. Amer. Math. Soc. **68** (1950) 337–404
14. Schoenberg, J.: Metric spaces and completely monotone functions. Ann. of Math. **39** (1938) 811–841
15. Azencott, R., Glowinski, R., He, J., Hoppe, R., Jajoo, A., Li, Y., Martynenko, A., S. Ben Zekry, M., S.H. Little, M., W. Zoghbi, M.: Diffeomorphic matching and dynamic deformable surfaces in 3d medical imaging. (2010) Comput. Meth. in Appl. Math., submitted.
16. Azencott, R., Glowinski, R., Ramos, A.: A controllability approach to shape identification. Applied Math. Letters **21** (2008) 861–865
17. Azencott, R., Alexander, S., Aggarwal, A., Jajoo, A., Jain, S., Li, Y., S. Ben Zekry, M., S.H. Little, M., W. Zoghbi, M.: New parameters to compare mitral annulus shapes extracted from 3d-echocardiography. (2010) submitted.
18. Azencott, R., Jajoo, A., Jain, S., Li, Y., Martynenko, A., S. Ben Zekry, M., S.H. Little, M., W. Zoghbi, M.: 3d-echocardiographic movies analysis: dynamic deformable models for mitral valve. (2010) submitted.